ACS Synthetic Biology

pubs.acs.org/synthbio

Letter

Synthetic Translational Regulation by Protein-Binding RNA Origami Scaffolds

Michael T. A. Nguyen, Georgios Pothoulakis, and Ebbe S. Andersen*

Cite This: *ACS Synth. Biol.* 2022, 11, 1710–1718

Read Online

ACCESS | Metrics & More | Article Recommendations | Supporting Information

ABSTRACT: Rational design approaches for the regulation of gene expression are expanding the synthetic biology toolbox. However, only a few tools for regulating gene expression at the translational level have been developed. Here, we devise an approach for translational regulation using the MS2 and PP7 aptamer and coat-protein pairs in *Escherichia coli*. The aptamers are used as operators in transcription units that encode proteins fused to their cognate coat proteins, which leads to self-repression. RNA origami scaffolds that contain up to four aptamers serve as an alternate binder to activate translation. With this system, we demonstrate that the increase in expression of a reporter protein is dependent on both the concentration and number of aptamers on RNA origami scaffolds. We also demonstrate regulation of multiple proteins using a single MS2 coat protein fusion and apply this method to regulate the relative expression of enzymes of the branched pathway for deoxyviolacein biosynthesis.

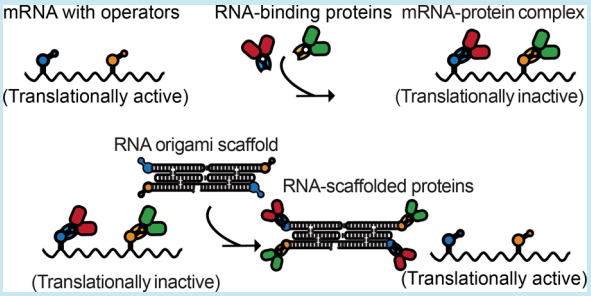

KEYWORDS: *RNA synthetic biology, RNA-protein complexes, post-transcriptional regulation, RNA origami*

INTRODUCTION

Synthetic biology aims to develop novel and robust tools to engineer biology, which have been achieved by mining, characterization, and adaptation of genetic parts for the creation of genetic circuits that perform various types of regulatory functions.[1,2] Recently, new RNA tools based on the *de novo* design principles have been emerging, enabling the creation of more advanced RNA-based regulators that control transcription[3,4] or translation.[5,6] *De novo* design has also been used to create RNA scaffolds for organizing molecular components, e.g., the RNA origami method that allows the design of single-stranded RNA nanostructures that can fold cotranscriptionally and thus can be genetically encoded and expressed in cells.[7,8] RNA origami has been applied to design RNA nanostructures that can spatially organize two light-up RNA aptamers to obtain Förster resonance energy transfer (FRET) in *Escherichia coli* (*E. coli*).[9] Furthermore, the production of wire-frame single-stranded RNA nanostructures in *E. coli* has been demonstrated.[10] RNA nanostructures can be utilized to organize protein-binding aptamers to colocalize recombinant proteins in cell-free expression systems[11] and to function as enzyme scaffolds that increase enzyme cascade reactions in *E. coli*.[12,13] RNA scaffolds have been fused to guide RNAs that, by means of endonuclease-dead Cas9, are brought to promoter sites where the scaffold can bind transcription factors for the transcriptional control of enzyme expression.[14,15] RNA scaffolding can be used to improve the folding, function, and stability of aptamers in comparison to aptamers separated by single-stranded linkers[11,14,16] but can also be used for precise spatial positioning of functional elements[13] and for implementation of conformational switches and devices.[9]

The RNA synthetic biology toolbox has furthermore been expanded with the use of protein-binding RNA motifs together with their cognate RNA-binding proteins (RBPs). Examples include the well-characterized coat proteins (CP) from the PP7 or MS2 single-stranded RNA bacteriophages, where MS2-CP (MCP) binds the MS2-hairpin (MS2hp)[17,18] and PP7-CP (PCP) binds the PP7-hairpin (PP7hp)[19,20] with high specificity and affinity. The binding of CPs to cognate RNA aptamers has been used to develop several translational repression systems.[17,19,21] Other examples are the utilization of the ribosomal protein L7 and the RNA kink-turn motif to create a translational switch[22] and the use of the CRISPR effector Cas6f as an insulator for predictable programming of gene expression through cleavage of its cognate RNA motif that can be placed between genes in a multicistronic transcription unit.[23] In nature, RNA regulators are usually associated with cognate RBPs that regulate several different genes post-transcriptionally.[24] For instance, carbon storage protein A (CsrA) acts as a global regulator of metabolism in *E. coli* by modulating the expression of various genes through binding of RNA motifs found in the

Received: December 7, 2021
Published: April 19, 2022

https://doi.org/10.1021/acssynbio.1c00608
ACS Synth. Biol. 2022, 11, 1710–1718

untranslated regions (UTR) in those genes. The activity of CsrA is further regulated by small RNA (sRNA) regulators CsrB and CsrC, that act as decoy RNA by having multiple CsrA-binding sites.[25,26] Engineering of this regulation system has been used for remodeling of cellular metabolism in *E. coli* through overexpression of CsrB to increase production of total free fatty acids.[27] Other examples of sRNA systems used for metabolic engineering include using the Hfq regulation system to create combinatorial libraries of sRNAs that target various genes to increase tyrosine and cadaverine biosynthesis in *E. coli*.[28]

Here, inspired by the biological function of MCP and PCP as translational repressors,[17,19] we designed a synthetic translational regulation system based on RNA−protein binding interactions of MS2hp−MCP and PP7hp−PCP. We show that this system leads to self-repression of the reporter protein and that it can be relieved by the expression of an RNA scaffold that binds to the repressor protein domain. The system is shown to be dependent on the concentration of the RNA scaffold and the number of aptamers on the RNA scaffold. We also demonstrate that control of the relative expression levels between two proteins is possible with the use of a single RNA scaffold that contains different combinations of MS2hp and PP7hp. Furthermore, we demonstrate that MCP can be used to repress another protein with an MS2 operator and that an MS2hp-containing RNA scaffold will be able to activate gene expression, which is finally used for directing the flux of the deoxyviolacein biosynthesis pathway.[29]

RESULTS AND DISCUSSION

Design of Genetic Circuits with Synthetic Translational Regulation. A synthetic translation regulation system was developed to control the expression of a protein by the expression of an RNA scaffold (Figure 1A). The system contains two divergent transcription units to avoid any read-through interference. One transcription unit was placed under an arabinose-inducible pBAD promoter and contains an mRNA encoding mScarlet fused to MCP with an MS2hp operator incorporated 4 bps downstream of the start codon, which has been shown to be the optimal spacing for translational repression when the site is bound by MCP[21] (Figure 1A, right). This construction results in self-repression, since the expression of mScarlet-MCP results in binding to the MS2hp operator, which blocks translation of mScarlet-MCP (Figure 1B, top). The other transcription unit was placed under control of the T7 promoter and contains an RNA scaffold with multiple MS2hps (Figure 1A, left). When expressed, the RNA scaffold will compete for binding to mScarlet-MCP, and when enough RNA scaffold is present, the equilibrium removes mScarlet-MCP from the MS2hp operator to allow mScarlet-MCP to be translated (Figure 1B, bottom). A similar system was made for the PCP/PP7hp pair. The insertion of the 4-bp spacer and the aptamer in the coding region results in the synthesis of small leader peptides of 8 and 10 amino acids for the MS2hp and PP7hp, respectively (see links to plasmid sequences in Table S1).

To test the effect of aptamer/protein-binding strengths, we used the aptamer variants MS2wt, MS2-G, PP7wt, and PP7-G (Figure S1), which have been reported to bind their cognate CPs with effective dissociation constants of 0.115, 0.33, 0.24, and 0.375, respectively.[21] The RNA scaffolds were designed based on the RNA origami method for generation of cotranscriptionally folded RNA nanostructures[7] that, due to their highly structured nature, can exhibit enhanced cellular stability[30] and improve aptamer functionality.[9,16] Using RNA origami design software tools, we generated RNA scaffolds with three parallel helix segments and added up to four aptamers on terminal-loop positions[8] (Figure S2). We decorated the RNA scaffolds with PP7wt and MS2wt aptamers, since these have the strongest protein binding affinity.[21] To ensure consistency across the scaffolds we first designed a scaffold with two MS2 and two PP7 aptamers (3H-2xMS2−2xPP7) using the RNA origami design software and used this as a backbone for the subsequent designs by exchanging the aptamers manually without performing additional sequence optimization and design. We also made a negative control scaffold with no operators/aptamers (3H-NO). We used the T7 expression system to ensure a high production of the RNA origami scaffolds, which is needed to achieve high-fold activation compared to when constitutive *E. coli* RNAP-driven promoters are used, as demonstrated in prior studies.[5,31] Therefore, the RNA origami scaffold designs were optimized for expression from a T7 promoter by including the transcription start sequence GGAA as part of their structure in the 5′-end. The genetic circuits were constructed by the EcoFlex MoClo toolkit[32] (see links to plasmid sequences in Table S1).

Translational Regulation with RNA Scaffolds Is Concentration- and Aptamer-Copy-Number-Dependent. The genetic circuit was expressed in *E. coli* using arabinose-containing media to express the mRNA transcription unit constitutively. Afterward, isopropyl-β-D-thiogalactoside (IPTG) was added to induce T7 RNA polymerase (RNAP) that drives the expression of the RNA scaffold, and the fluorescence output was evaluated by flow cytometry (see histograms in Figures S3 and S4). To investigate the effect of RNA scaffold concentration, we measured the mScarlet-I fluorescence with increasing concentrations of IPTG. We observe a small decrease of mScarlet-I expression when inducing T7 RNAP expression, which is likely due to the sharing of metabolic resources for protein expression (raw data in Figure S5). We therefore used fold-activation of mScarlet-I expression to measure the effect of the RNA scaffolds as translational activators. The fold-activation was calculated by normalizing the reporter expression levels from an aptamer-containing RNA scaffold to those obtained from the control RNA origami scaffold carrying no aptamers (3H-NO).

For the PP7wt operator, we observed that mScarlet-PCP expression increased with increasing IPTG concentration only when aptamers were present on the scaffold (Figure 1C left and S3). With one PP7wt aptamer on the RNA scaffold, mScarlet-I-PCP reached 5-fold activation, and with four aptamers on the RNA scaffold it reached 10-fold activation (Figure 1C left). Under the PP7-G operator, mScarlet-I-PCP expression reached a plateau of 2.5-fold activation at 100 μM IPTG when expressing an RNA scaffold with one PP7wt aptamer (Figure 1C right). With a four-aptamer RNA scaffold, the mScarlet-I-PCP expression reached a plateau of 4-fold activation at 20 μM IPTG (Figure 1C right).

For the MS2wt operator, we observed an initial increase followed by a decrease in mScarlet-I-MCP expression (Figures 1D, left, and S4). Expression of an RNA scaffold with one or four MS2 aptamers resulted in a maximum activation of 6-fold and 10-fold at 20 μM IPTG, respectively (Figure 1D left). For the MS2-G operator, we observed that one MS2 aptamer resulted in 5-fold activation and four MS2 aptamers resulted in 9-fold activation at 100 μM IPTG (Figure 1D right). A comparison of the absolute mean fluorescence between the different strains at 20 μM IPTG revealed that MS2wt and PP7wt in general

https://doi.org/10.1021/acssynbio.1c00608
ACS Synth. Biol. 2022, 11, 1710−1718

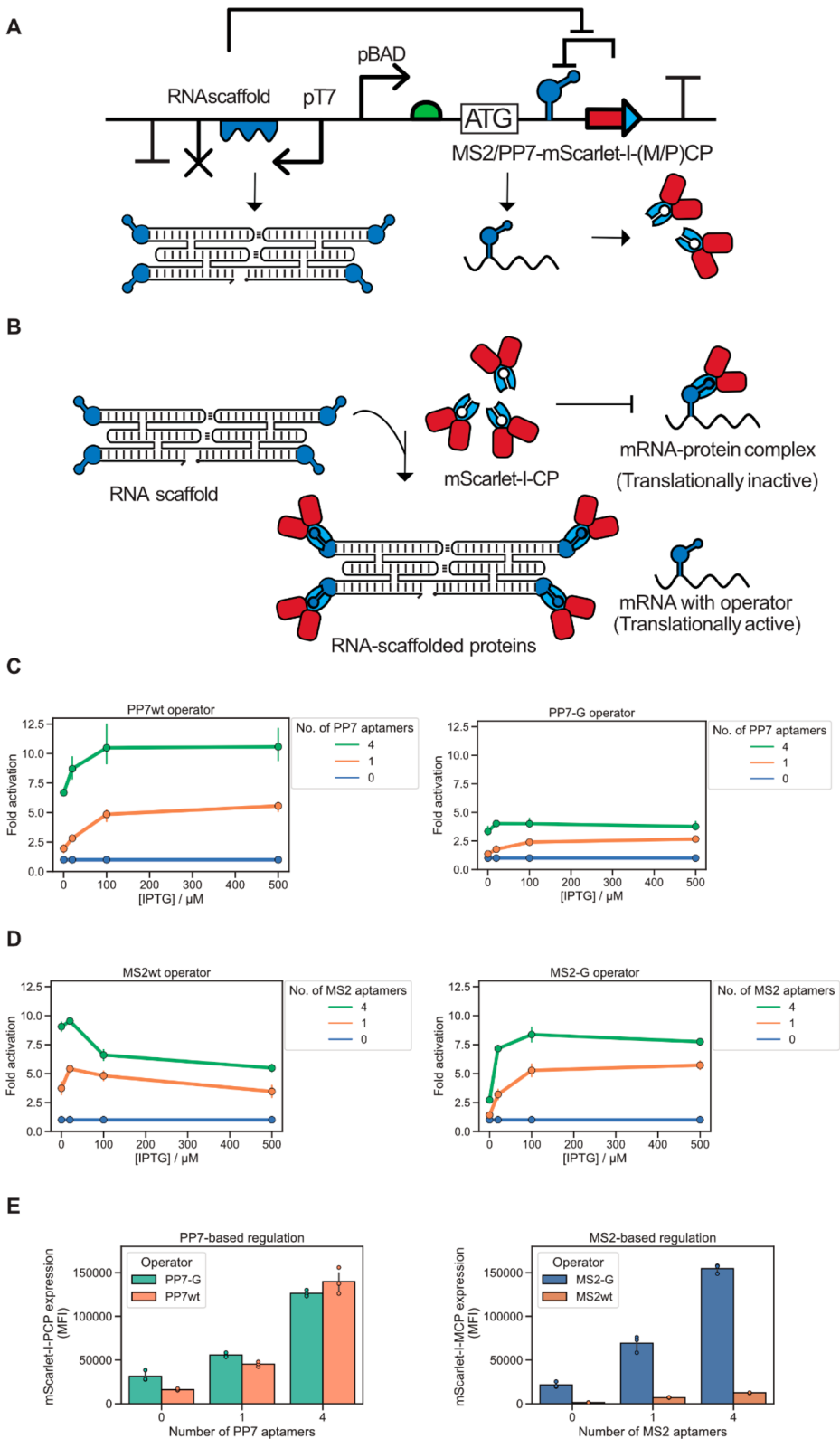

Figure 1. RNP-based synthetic translational regulation by MS2 or PP7 proteins. (A) Genetic circuit diagram for RNP-based regulation. The left transcription unit consists of an ncRNA scaffold (wavy object) under the control of the T7 promoter (arrow), an HDV56 ribozyme (line with X), and a T7 terminator (large "T"). The right transcription unit contains a coding sequence for mScarlet-I fused with a phage coat protein under the control of the pBAD promoter (arrow) and an RBS (half-circle) with a cognate RNA aptamer that acts as an operator (stem loop). (B) The RNA operator leads to self-repression when bound by the phage coat protein, which is alleviated by expression of an RNA scaffold with competing aptamer domains. (C,D) Flow cytometry analysis of translational regulation with PP7-PCP or MS2-MCP. (E) Absolute expression values of mScarlet-I-(M/P)CP for all four operator variants at 20 μM IPTG. Mean fluorescence intensity (MFI) is calculated as geometric means of mScarlet-I fluorescence. All error bars denote standard deviation from triplicate measurements.

https://doi.org/10.1021/acssynbio.1c00608
ACS Synth. Biol. 2022, 11, 1710−1718

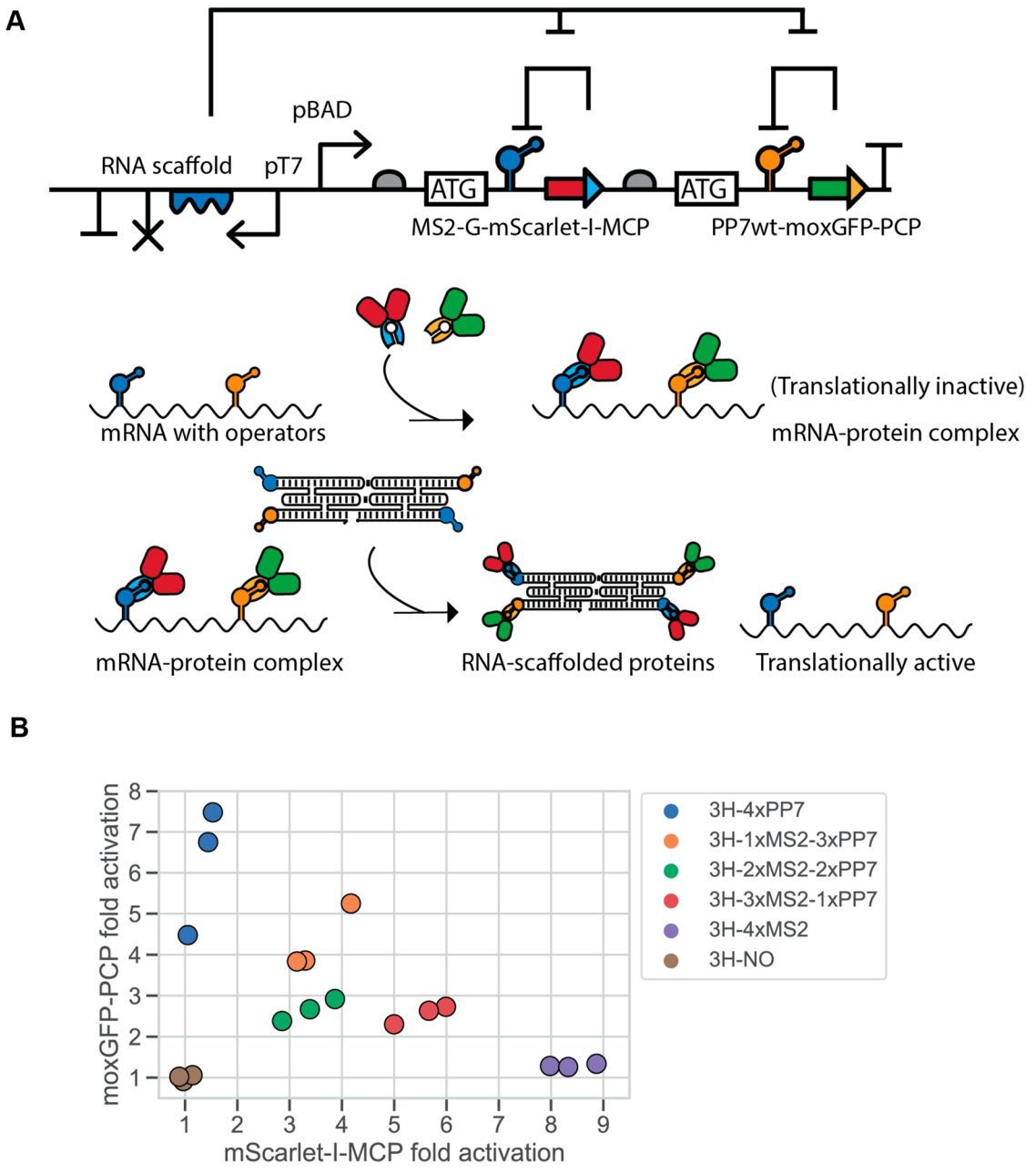

Figure 2. MS2 and PP7 aptamer copy number determine relative protein expression. (A) Genetic circuit diagram for coexpression of two CP-tagged proteins with a single RNA scaffold. Transcription units are placed divergently from each other. The RNA transcription unit consists of an RNA scaffold under the control of the T7 promoter, an HDV56 ribozyme and T7 terminator. The protein transcription contains mScarlet-I fused with a phage coat protein under the control of the pBAD promoter. Downstream, the RBS is a cognate RNA hairpin operator. Same symbols as in Figure 1. (B) Scatter plot of the fold-change in reporter protein expression normalized to average values of reporters coexpressed with negative control RNA 3H-NO from triplicate measurements induced with 20 μM IPTG. Individual values from the triplicates are shown.

exhibited lower expression compared to the mutant variants (Figure 1E), which is explained by their stronger binding affinity.[21]

We observed that basal expression of a scaffold with four aptamers led to high basal activation, which might be an issue if tight control of gene expression is needed. This was shown to be reduced by 2-fold by coexpression of the T7 lysozyme, which is a natural inhibitor of T7 RNAP[33] (Figures S6 and S7). However, T7 lysozyme coexpression also led to an overall decrease in expression and less potent activation, and we therefore did not use the T7 lysozyme for leakage reduction. Another strategy to reduce transcriptional leakage could be the addition of the lac operator to the T7 promoter in conjunction with expression of the lac repressor. However, this would require a redesign of the RNA origami scaffolds to include the downstream operator sequence into their structure.

We conclude that the RNA scaffolds act as translational regulators by competing with operator binding to cognate CP and that the protein expression is dependent both on RNA-scaffold concentration and on the numbers of aptamers on the scaffold and binding strength.

Orthogonal and Stoichiometric Control of Protein Expression. We further explored the possibility of combining both MS2 and PP7 operators on a bicistronic genetic construct

https://doi.org/10.1021/acssynbio.1c00608
ACS Synth. Biol. 2022, 11, 1710−1718

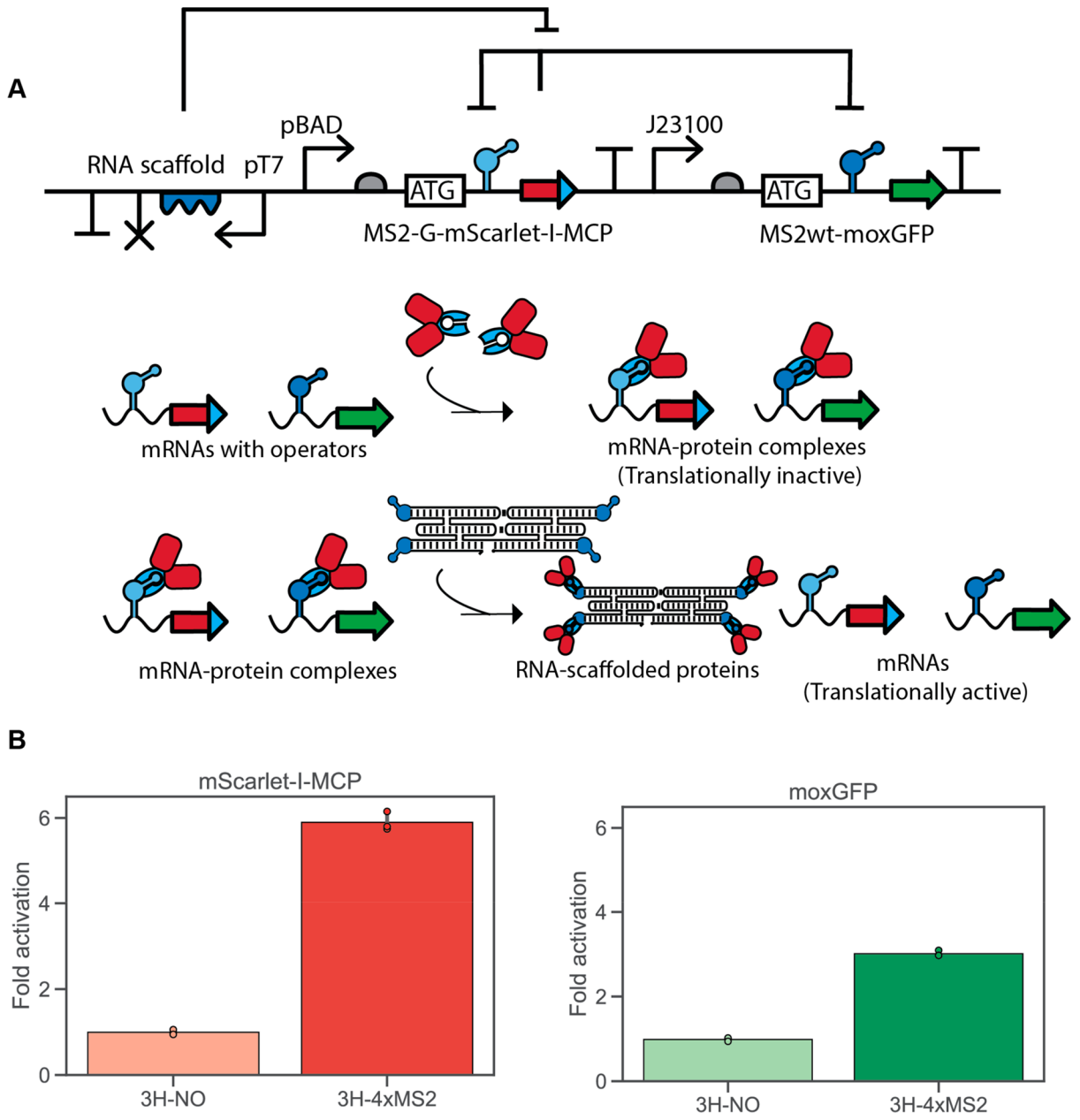

Figure 3. Regulation of multiple protein targets from a single type RNA scaffold. (A) Genetic circuit diagram for regulation of multiple proteins using the MS2-MCP system. Expression of mScarlet-I-MCP leads to repression of MS2hp-tagged moxGFP, which can be alleviated with an RNA scaffold. Same symbols as in Figure 1. (B) Normalized expression of mScarlet-I-MCP (left) and moxGFP (right) compared to expression levels with the negative control 3H-NO from three replicates.

as a two-protein system with orthogonal control of two different reporter proteins, moxGFP−PCP and mScarlet-I−MCP (Figure 2A). We chose the MS2-G and PP7wt as operators since they exhibited similar reporter expression levels with low basal expression (Figure 1E). In addition, we designed RNA scaffolds each containing four aptamers with the different possible combinations of the two aptamers MS2wt and PP7wt, thus ending up with five different scaffolds: 4xMS2, 4xPP7, 3xMS2−1xPP7, 1xMS2−3xPP7, and 2xMS2−2xPP7 (Figure S2). Expression was analyzed by flow cytometry (histograms are shown in Figure S8).

Expression of a scaffold with four copies of either MS2wt or PP7wt aptamers leads to increased expression of the cognate reporter protein by up to 8-fold compared to the negative control with no fold-activation of the noncognate reporter protein (Figure 2B, blue and purple data points). Expressing an RNA scaffold with three copies of the MS2wt aptamer and one copy of the PP7wt aptamer resulted in up to a 6-fold increase in mScarlet-I-MCP and a up to 3-fold increase of moxGFP-PCP (Figure 2B, red data points). Expression of a scaffold with three PP7wt aptamers and one MS2wt aptamer led up to a 5-fold increase of moxGFP-PCP and up to a 4-fold increase of mScarlet-I-MCP (Figure 2B, orange data points). Expression of a scaffold with two of each aptamer resulted in up to a 4-fold increase of mScarlet-I-MCP and up to a 3-fold increase of moxGFP-PCP (Figure 2B, green data points). Surprisingly, a scaffold with two MS2wt aptamers and two PP7wt aptamers demonstrated the same fold activation of mScarlet-I-MCP and moxGFP-PCP as a scaffold with either one MS2 or one PP7 aptamer, respectively. The apparent lower expression level of

https://doi.org/10.1021/acssynbio.1c00608
ACS Synth. Biol. 2022, 11, 1710−1718

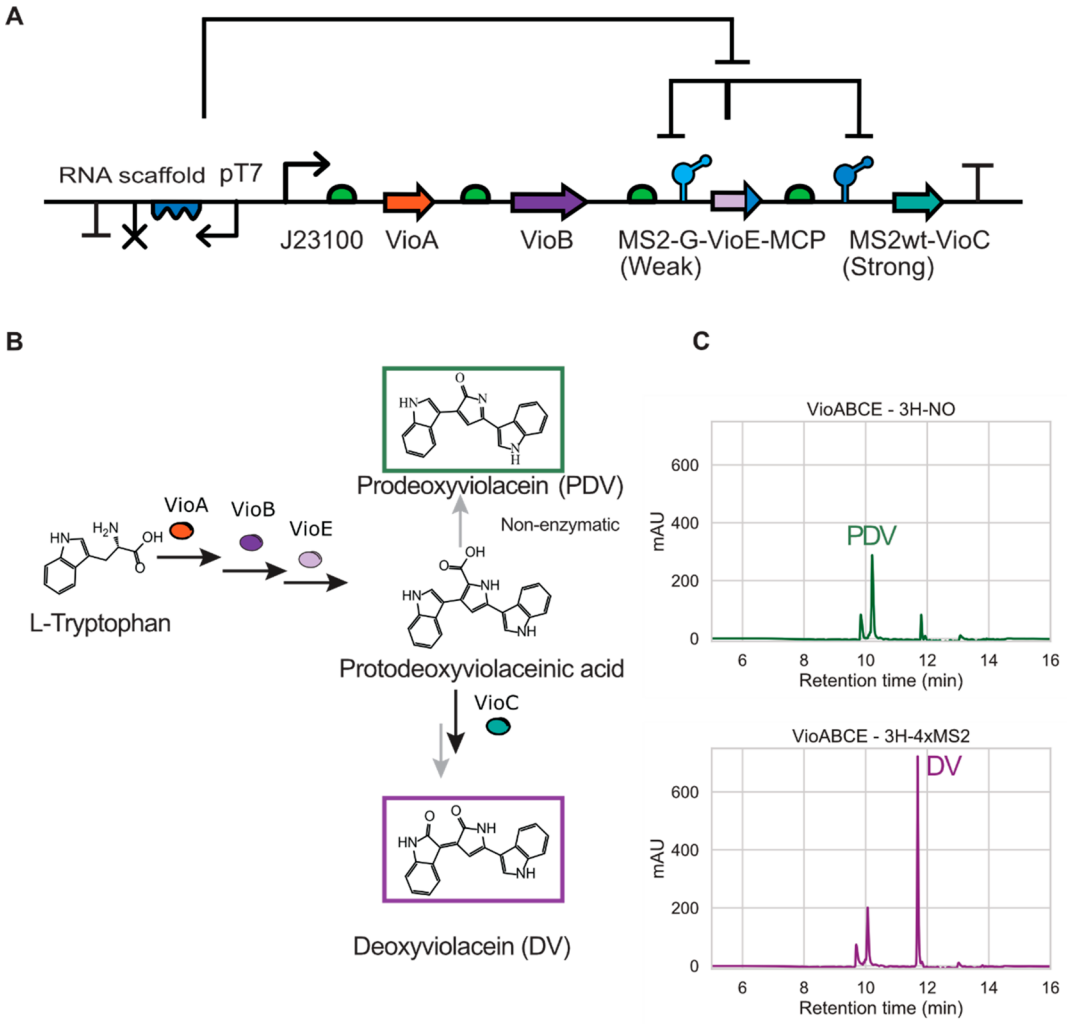

Figure 4. Synthetic translational regulation of the deoxyviolacein pathway for flux redirection. (A) Genetic circuit diagram of the pathway design. Same symbols as in Figure 1. (B) Deoxyviolacein pathway. L-Tryptophan is converted to protodeoxyviolaceinic acid via VioA, VioB, and VioE, which subsequently can be nonenzymatically converted to prodeoxyviolacein (gray arrow) or enzymatically converted to deoxyviolacein via VioC (black arrow) and a nonenzymatic step (gray arrow). (C) HPLC chromatograms of biosynthesis of PDV and DV with coexpression of the pathway with the 3H-NO RNA scaffold (top) and a strain coexpressing the pathway with the 3H-4xMS2 RNA scaffold (bottom).

this construct could be caused by misfolding of the aptamers, sterical effects of multiple protein binding, or an effect from bicistronic expression. We do not think it is caused by misfolding, since this construct (3H−2xMS2−2xPP7) was the initially designed scaffold that was used to construct the other scaffolds. We also do not think this is caused by sterical effects, since the RNA origami scaffolds were designed with a spacing between the aptamers that should allow full occupancy.[8] We however do think this could be due to a synergistic effect caused by having the two proteins expressed from a bicistronic mRNA. High expression for one protein, i.e., when activated by an RNA scaffold with at least three aptamers, could stabilize the mRNA, compared to when RNA scaffolds with only two aptamers are expressed, and therefore cause an increase in expression for the other protein that is activated by a scaffold. We also observed a linear trend between each individual replicate for each strain, which could indicate that the main variable of variance is the level of RNA scaffold expression. Our results show that it is possible to control protein expression stoichiometry with an RNA scaffold based on the available binding sites.

Regulation of Multiple Proteins Using Aptamer-Based Operators. Next, we sought to use the MS2−MCP pair to regulate multiple proteins by a single type of RNA scaffold. By taking advantage of the MS2 aptamer's ability to bind any MCP-tagged protein, we incorporated an MS2 operator onto a transcription unit with moxGFP that could be regulated by mScarlet-I-MCP, essentially utilizing it as a modular subgene biopart to regulate the translation of other genes. To ensure tight repression by mScarlet-I-MCP, we placed moxGFP under the strong operator MS2wt and mScarlet-I-MCP under the weaker operator MS2-G. Since MS2wt has a stronger protein-binding affinity, we expect this operator site to be favored for binding of mScarlet-I-MCP, thus moxGFP will be more tightly repressed. Expression of mScarlet-I-MCP leads to self-repression and repression of moxGFP that would be alleviated in the presence of an RNA scaffold with MS2 aptamers (Figure 3A). Expression of an RNA scaffold with four copies of the MS2 aptamers led to a 6-fold activation of the regulator mScarlet-I-MCP and a 3-fold activation of the reporter moxGFP, thus confirming our hypothesis about tighter repression of moxGFP (Figure 3B and Figure S9). These results show that it is possible to use the operator as a modular part to translationally regulate multiple proteins and control the relative expression levels of multiple proteins through autoregulatory means rather than tuning the

https://doi.org/10.1021/acssynbio.1c00608
ACS Synth. Biol. 2022, 11, 1710−1718

promoter or RBS. Furthermore, an RNA scaffold can be expressed to activate the gene expression, creating an RNA master regulator.

RNA Scaffolds Control Metabolic Flux of Deoxyviolacein. To demonstrate an application of our synthetic RNA−protein regulation system, we applied the MS2−MCP regulation strategy to control flux of the four-enzyme pathway for deoxyviolacein biosynthesis that consists of VioA, VioB, VioC, and VioE.[29] We fused VioE to MCP and placed an MS2wt operator on the VioC gene and an MS2-G operator on the VioE-MCP gene. This would allow VioE-MCP to exhibit control of the expression of VioC and direct the flux of the pathway (Figure 4A). Deoxyviolacein biosynthesis starts with L-tryptophan to produce protodeoxyviolaceinic acid by VioA, VioB, and VioE (Figure 4B). Subsequent nonenzymatic decarboxylation leads to the conversion of prodeoxyviolacein (PDV). Protodeoxyviolaceinic acid is also a substrate for VioC, and it is used to synthesize deoxyviolacein (DV).

Expression of the modified pathway led to the accumulation of PDV as the dominant product, likely due to a repressed VioC caused by VioE-MCP. The coexpression of a decoy RNA with MS2 aptamers shifted the metabolic flux and resulted in DV being the main product through the translational activation of VioC and VioE-MCP (Figure 4C). The ratios between PDV and DV peak areas were found to be 0.7 ± 0.6 and 3.0 ± 1.7, when expressed with a negative control RNA and a scaffold with four MS2 aptamers, respectively (Figure S10). With this, we have shown functionalization of a biosynthetic enzyme as a translational regulator, through the simple fusion with MCP and addition of MS2 operators at several positions at the gene cassette, to regulate the relative expression levels of enzymes and thus direct the metabolic flux. Overall, this is a new strategy for balancing pathway-related enzymes and could be used as tool for metabolic engineering, where relative expression is crucial for optimal flux.

CONCLUSIONS

We have demonstrated the design and viability of a translational regulation system based on the utilization of the known RNA−protein binding pairs, MS2hp−MCP and PP7hp−PCP. This system can be used as a method for efficient and conditional coexpression of RNA−protein complexes and as an RNA scaffold-dependent regulation tool. With the design of a bicistronic genetic construct, we were able to show control of relative protein expression based on RNA aptamer combinations on a single RNA scaffold. This method could potentially also be used as a coexpression strategy for optimizing RNA−protein complex assembly by matching the production and demand of RNA and protein components since the proteins that can be scaffolded are autoregulated and thus only will be expressed when RNA scaffolds are present. This reduces the need for tuning the expression of each component to ensure optimal scaffolding. Thus, we expect that this regulation system can be used to enable robust and stoichiometric assembly of multifunctional RNA−protein scaffold complexes in cells without excessive expression of either component. We further extended the system by fusing an MCP domain to another reporter protein, which made it possible to add additional regulatory functionality and also modulate the activation with a decoy RNA containing MS2 aptamers. This strategy was applied to control the flux of the deoxyviolacein metabolic pathway by balancing the enzyme expression using an RNA master regulator, and we ultimately propose this decoy-based method that controls relative protein expression as a valuable addition to the synthetic biology toolbox for RNA-based regulation of gene expression.

MATERIALS AND METHODS

RNA Scaffold Design. Blueprints were constructed manually for compatibility with the RNA origami automated design software suite.[8] Sequences were designed using the Revolvr software to generate 20 sequences that were evaluated by ensemble defect. The RNA designs with the lowest ensemble defect score were chosen.

Plasmid Assembly and *E. coli* Strain Creation. Plasmid propagation was performed in NEB Turbo cells. For selection, lysogeny broth (LB) media and agar plates containing either 100 μg/mL carbenicillin or 34 μg/mL chloramphenicol were used.

Part plasmids were generated from synthesized double stranded DNA fragments (Twist Bioscience or Integrated DNA Technologies). The synthesized gene fragments carried flanking sequences containing the appropriate pre- and suffixes for correct assembly into transcription units following a modified EcoFlex MoClo toolkit method.[32] Golden Gate reactions were performed with equimolar amounts of DNA using 25 femtomoles of DNA, 0.25 μL of T4 DNA ligase, 0.5 μL of either Esp3I, or BsaI in 1× T4 DNA ligase buffer with 10 μM ATP in 5 μL reactions. Golden Gate reactions consisted of 10 min at 37 °C, followed by nine cycles of 3 min at 37 °C and 4 min at 16 °C followed by heat-inactivation of the enzymes by a 5 min incubation at 50 °C and at 80 °C. Sequence-verified part plasmids were used for the assembly of single gene cassettes using a Golden Gate protocol with BsaI. Gene and multigene cassettes were verified by restriction analysis using either Esp3I or BsaI, respectively.

For the assembly of bicistronic and DV pathway cassettes, part plasmids were used in a a Golden Gate reaction together with unique nucleotide sequence (UNS) adapters[34] modified for the EcoFlex MoClo toolkit[32] and assembled using a Golden Gate protocol similar to the above with only five cycles of thermal cycling. The Golden Gate reaction mixes were then directly used as templates for PCR using Q5 DNA polymerase (NEB) and UNS primers. Thermocycling was performed according to a standard Q5 PCR protocol with annealing at 64 °C. Desired PCR products were purified by gel extraction using a NucleoSpin Gel and PCR purification kit (Macherey-Nagel). PCR products were then used in a Gibson assembly reaction with a mix made in-house.[35] Correctly assembled plasmids were verified by Sanger sequencing (Eurofins Genomics).

Growth and Expression Conditions for Flow Cytometry. Multigene cassette plasmids were transformed into JM109 (DE3) for expression experiments and plated out on LB-agar selection plates containing 34 μg/mL chloramphenicol. Single colonies were picked and grown in 200 μL of nonphosphate buffered Terrific Broth (TB; yeast extract 24 mg/mL, peptone 20 mg/mL) supplemented with 34 μg/mL of chloramphenicol overnight in a 96-deep-well plate (Abgene) at 37 °C with shaking at 900 rpm on a Thermomixer C (Eppendorf). After overnight growth, the cells were back-diluted 1:100 in 400 μL of chloramphenicol-supplemented TB with the addition of 0.2% L-arabinose and grown for 2 h. 200 μL of the cells were induced with various IPTG concentrations (0, 20, 100, 500 μM) for the single-protein cassettes and 20 μM for the two-protein cassettes. The cells were then grown for an additional 4 h before flow cytometry acquisition in a Novocyte flowcytometer.

https://doi.org/10.1021/acssynbio.1c00608
ACS Synth. Biol. 2022, 11, 1710−1718

Bioproduction and Extraction of Deoxyviolacein Products. Single colonies were inoculated in 2 mL of TB-chloramphenicol in a 14 mL Falcon tube and grown for 48 h at 37 °C with shaking at 230 rpm. Then, 500 μL of the cell cultures were harvested by centrifugation at 17 000*g* for a minute in a table top centrifuge. After removal of the supernatant, the cell pellets were lysed in 200 μL of methanol, boiled at 95 °C for 5 min, and cell debris was pelleted by centrifugation at 17 000*g*. 150 μL of the supernatant was filter-sterilized using a 0.22 μm filter before HPLC analysis.

For HPLC measurements, 100 μL of sample (50/50 of water + extract) was run on an Agilent 1200 Series LC system using an Agilent Extend-C18 column (150 × 4.6 mm, 3.5 μm). Solvent A (0.1% formic acid in water) and solvent B (0.1% formic acid in acetonitrile) were used as follows: start at 5% solvent B, 5% solvent B for 2 min, transition to 98% solvent B (9.3%/min), transition to 5% solvent B (31%/min), and hold for 3 min (this method is adjusted from a prior protocol by Lee et al.[36]). The flow rate was 500 μL/min, the column temperature at 30 °C, and absorbance was measured at 260 nm, 220 nm, 565 nm (reported in the results), and 600 nm using a UV/vis detector. A violacein/deoxyviolacein mixed extract (Sigma-Aldrich) was used as a reference. The peak areas for the respective compounds were used for the relative quantification.

■ ASSOCIATED CONTENT

Supporting Information

The Supporting Information is available free of charge at https://pubs.acs.org/doi/10.1021/acssynbio.1c00608.

Secondary structure diagrams of RNA hairpins and RNA origami scaffolds, representative flow cytometry histograms, additional flow cytometry data, T7 Lysozyme coexpression data, quantification of PDV/DV ratio, list of plasmid and primer sequences (PDF)

■ AUTHOR INFORMATION

Corresponding Author

Ebbe S. Andersen − *Interdisciplinary Nanoscience Center, Aarhus University, 8000 Aarhus C, Denmark; Department of Molecular Biology and Genetics, Aarhus University, 8000 Aarhus C, Denmark;* orcid.org/0000-0002-6236-8164; Phone: +45 41178619; Email: esa@inano.au.dk

Authors

Michael T. A. Nguyen − *Interdisciplinary Nanoscience Center, Aarhus University, 8000 Aarhus C, Denmark*

Georgios Pothoulakis − *Interdisciplinary Nanoscience Center, Aarhus University, 8000 Aarhus C, Denmark*

Complete contact information is available at: https://pubs.acs.org/10.1021/acssynbio.1c00608

Author Contributions

M.T.N. conceived, designed, and performed the experiments. G.P. and E.S.A. supervised the research. All authors discussed and wrote the paper.

Notes

The authors declare no competing financial interest.

■ ACKNOWLEDGMENTS

This project was financed by a European Research Council Consolidator Grant (RNA ORIGAMI—RNA-protein nanostructures for synthetic biology, 683305) and a Novo Nordisk Foundation Ascending Investigator Grant (0060694). We thank Cody Geary for assistance on using Revolr for RNA scaffold design and Richard Murray and Elisa Franco for discussions. Thanks to Rita Rosendahl and Claus Bus for technical assistance. The EcoFlex kit used for cloning was a gift from Paul Freemont (Addgene kit #1000000080).

■ REFERENCES

(1) Brophy, J. A. N.; Voigt, C. A. *Principles of genetic circuit design* **2014**, *11*, 508−520.

(2) Nielsen, A. A. K.; Der, B. S.; Shin, J.; Vaidyanathan, P.; Paralanov, V.; Strychalski, E. A.; Ross, D.; Densmore, D.; Voigt, C. A. Genetic circuit design automation. *Science* **2016**, *352*, aac7341.

(3) Chappell, J.; Takahashi, M. K.; Lucks, J. B. Creating small transcription activating RNAs. *Nat. Chem. Biol.* **2015**, *11*, 214−220.

(4) Chappell, J.; Westbrook, A.; Verosloff, M.; Lucks, J. B. Computational design of small transcription activating RNAs for versatile and dynamic gene regulation. *Nat. Commun.* **2017**, *8*, 1051.

(5) Green, A. A.; Kim, J.; Ma, D.; Silver, P. A.; Collins, J. J.; Yin, P. Complex cellular logic computation using ribocomputing devices. *Nature* **2017**, *548*, 117−121.

(6) Kim, J.; Zhou, Y.; Carlson, P. D.; Teichmann, M.; Chaudhary, S.; Simmel, F. C.; Silver, P. A.; Collins, J. J.; Lucks, J. B.; Yin, P.; Green, A. A. De novo-designed translation-repressing riboregulators for multi-input cellular logic. *Nat. Chem. Biol.* **2019**, *15*, 1173−1182.

(7) Geary, C.; Rothemund, P. W. K.; Andersen, E. S. A single-stranded architecture for cotranscriptional folding of RNA nanostructures. *Science* **2014**, *345*, 799−804.

(8) Geary, C.; Grossi, G.; McRae, E. K. S.; Rothemund, P. W. K.; Andersen, E. S. RNA origami design tools enable cotranscriptional folding of kilobase-sized nanoscaffolds. *Nat. Chem.* **2021**, *13*, 549−558.

(9) Jepsen, M. D. E.; Sparvath, S. M.; Nielsen, T. B.; Langvad, A. H.; Grossi, G.; Gothelf, K. V.; Andersen, E. S. Development of a genetically encodable FRET system using fluorescent RNA aptamers. *Nat. Commun.* **2018**, *9*, 1−10.

(10) Li, M.; Zheng, M.; Wu, S.; Tian, C.; Liu, D.; Weizmann, Y.; Jiang, W.; Wang, G.; Mao, C. In vivo production of RNA nanostructures via programmed folding of single-stranded RNAs. *Nat. Commun.* **2018**, *9*, 2196−2196.

(11) Schwarz-Schilling, M.; Dupin, A.; Chizzolini, F.; Krishnan, S.; Mansy, S. S.; Simmel, F. C. Optimized Assembly of a Multifunctional RNA-Protein Nanostructure in a Cell-Free Gene Expression System. *Nano Lett.* **2018**, *18*, 2650−2657.

(12) Delebecque, C. J.; Lindner, A. B.; Silver, P. A.; Aldaye, F. A. Organization of intracellular reactions with rationally designed RNA assemblies. *Science* **2011**, *333*, 470−474.

(13) Sachdeva, G.; Garg, A.; Godding, D.; Way, J. C.; Silver, P. A. In vivo co-localization of enzymes on RNA scaffolds increases metabolic production in a geometrically dependent manner. *Nucleic Acids Res.* **2014**, *42*, 9493−9503.

(14) Zalatan, J. G.; Lee, M. E.; Almeida, R.; Gilbert, L. A.; Whitehead, E. H.; La Russa, M.; Tsai, J. C.; Weissman, J. S.; Dueber, J. E.; Qi, L. S.; Lim, W. A. Engineering complex synthetic transcriptional programs with CRISPR RNA scaffolds. *Cell* **2015**, *160*, 339−350.

(15) Dong, C.; Fontana, J.; Patel, A.; Carothers, J. M.; Zalatan, J. G. Synthetic CRISPR-Cas gene activators for transcriptional reprogramming in bacteria. *Nat. Commun.* **2018**, *9*, 2489.

(16) Krissanaprasit, A.; Key, C.; Fergione, M.; Froehlich, K.; Pontula, S.; Hart, M.; Carriel, P.; Kjems, J.; Andersen, E. S.; LaBean, T. H. Genetically Encoded, Functional Single-Strand RNA Origami: Anticoagulant. *Adv. Mater.* **2019**, *31*, 1808262−1808262.

(17) Peabody, D. S. Translational repression by bacteriophage MS2 coat protein expressed from a plasmid. A system for genetic analysis of a protein-RNA interaction. *J. Biol. Chem.* **1990**, *265*, 5684−5689.

(18) Peabody, D. S. The RNA binding site of bacteriophage MS2 coat protein. *EMBO J.* **1993**, *12*, 595−600.

(19) Lim, F.; Downey, T. P.; Peabody, D. S. Translational repression and specific RNA binding by the coat protein of the Pseudomonas phage PP7. *J. Biol. Chem.* **2001**, *276*, 22507−22513.
(20) Chao, J. A.; Patskovsky, Y.; Almo, S. C.; Singer, R. H. Structural basis for the coevolution of a viral RNA-protein complex. *Nat. Struct Mol. Biol.* **2008**, *15*, 103−105.
(21) Katz, N.; Cohen, R.; Solomon, O.; Kaufmann, B.; Atar, O.; Yakhini, Z.; Goldberg, S.; Amit, R. An in Vivo Binding Assay for RNA-Binding Proteins Based on Repression of a Reporter Gene. *ACS Synth. Biol.* **2018**, *7*, 2765−2774.
(22) Saito, H.; Kobayashi, T.; Hara, T.; Fujita, Y.; Hayashi, K.; Furushima, R.; Inoue, T. Synthetic translational regulation by an L7Ae-kink-turn RNP switch. *Nat. Chem. Biol.* **2010**, *6*, 71−78.
(23) Qi, L.; Haurwitz, R. E.; Shao, W.; Doudna, J. A.; Arkin, A. P. RNA processing enables predictable programming of gene expression. *Nat. Biotechnol.* **2012**, *30*, 1002−1006.
(24) Waters, L. S.; Storz, G. Regulatory RNAs in Bacteria. *Cell* **2009**, *136*, 615−615.
(25) Liu, M. Y.; Gui, G.; Wei, B.; Preston, J. F., 3rd; Oakford, L.; Yuksel, U.; Giedroc, D. P.; Romeo, T. The RNA molecule CsrB binds to the global regulatory protein CsrA and antagonizes its activity in Escherichia coli. *J. Biol. Chem.* **1997**, *272*, 17502−17510.
(26) Weilbacher, T.; Suzuki, K.; Dubey, A. K.; Wang, X.; Gudapaty, S.; Morozov, I.; Baker, C. S.; Georgellis, D.; Babitzke, P.; Romeo, T. A novel sRNA component of the carbon storage regulatory system of Escherichia coli. *Mol. Microbiol.* **2003**, *48*, 657−670.
(27) McKee, A. E.; Rutherford, B. J.; Chivian, D. C.; Baidoo, E. K.; Juminaga, D.; Kuo, D.; Benke, P. I.; Dietrich, J. A.; Ma, S. M.; Arkin, A. P.; Petzold, C. J.; Adams, P. D.; Keasling, J. D.; Chhabra, S. R. Manipulation of the carbon storage regulator system for metabolite remodeling and biofuel production in Escherichia coli. *Microbial Cell Factories 2012 11:1* **2012**, *11*, 1−12.
(28) Na, D.; Yoo, S. M.; Chung, H.; Park, H.; Park, J. H.; Lee, S. Y. Metabolic engineering of Escherichia coli using synthetic small regulatory RNAs. *Nat. Biotechnol.* **2013**, *31*, 170−174.
(29) Balibar, C. J.; Walsh, C. T. In vitro biosynthesis of violacein from L-tryptophan by the enzymes VioA-E from Chromobacterium violaceum. *Biochemistry* **2006**, *45*, 15444−15457.
(30) Deutscher, M. P. How bacterial cells keep ribonucleases under control. *FEMS Microbiol Rev.* **2015**, *39*, 350−361.
(31) Green, A. A.; Silver, P. A.; Collins, J. J.; Yin, P. Toehold switches: De-novo-designed regulators of gene expression. *Cell* **2014**, *159*, 925.
(32) Moore, S. J.; Lai, H. E.; Kelwick, R. J.; Chee, S. M.; Bell, D. J.; Polizzi, K. M.; Freemont, P. S. EcoFlex: A Multifunctional MoClo Kit for E. coli Synthetic Biology. *ACS Synth. Biol.* **2016**, *5*, 1059−1069.
(33) Studier, F. W. Use of bacteriophage T7 lysozyme to improve an inducible T7 expression system. *J. Mol. Biol.* **1991**, *219*, 37.
(34) Halleran, A. D.; Swaminathan, A.; Murray, R. M. Single Day Construction of Multigene Circuits with 3G Assembly. *ACS Synth. Biol.* **2018**, *7*, 1477−1480.
(35) Gibson, D. G.; Young, L.; Chuang, R. Y.; Venter, J. C.; Hutchison, C. A., 3rd; Smith, H. O. Enzymatic assembly of DNA molecules up to several hundred kilobases. *Nat. Methods* **2009**, *6*, 343−345.
(36) Lee, M. E.; Aswani, A.; Han, A. S.; Tomlin, C. J.; Dueber, J. E. Expression-level optimization of a multi-enzyme pathway in the absence of a high-throughput assay. *Nucleic Acids Res.* **2013**, *41*, 10668−10678.

https://doi.org/10.1021/acssynbio.1c00608
ACS Synth. Biol. 2022, 11, 1710−1718